IEEE Access
Multidisciplinary | Rapid Review | Open Access Journal

Received December 25, 2018, accepted April 4, 2019, date of publication April 11, 2019, date of current version July 12, 2019.

Digital Object Identifier 10.1109/ACCESS.2019.2910735

SAR Image Segmentation Using Hierarchical Region Merging With Orientated Edge Strength Weighted Kuiper's Distance

ZEJUN ZHANG[1,2], XIONG PAN[1], LI CHENG[3], SHIHUA ZHAN[1,2], HUABING ZHOU[4], RIQING CHEN[1], CHANGCAI YANG[1], CHANGYING WANG[1], YAOHAI LIN[1], AND JIAXIANG LIN[1]

[1]The Digital Fujian Institute of Big Data for Agriculture and Forestry, College of Computer and Information Sciences, Fujian Agriculture and Forestry University, Fuzhou 350002, China
[2]Key Laboratory of Smart Agriculture and Forestry, Fujian Agriculture and Forestry University, Fujian Province University, Fuzhou 350002, China
[3]Jinshan College, Fujian Agriculture and Forestry University, Fuzhou 350002, China
[4]The School of Computer Science and Engineering, Wuhan Institute of Technology, Wuhan 430070, China

Corresponding author: Riqing Chen (riqing.chen@fafu.edu.cn)

This work was supported in part by the National Natural Science Foundation of China under Grant 61501120, Grant 61702101 and Grant 61701117, in part by the Natural Science Fund of Fujian Province under Grant 2016J01753, Grant 2017J01736, Grant 2018J01645, and Grant 2018J01644, in part by the Construction Fund for Digital Fujian Big Data for Agriculture and Forestry under Grant KJG18019A, in part by the Special Fund for Scientific and Technological Innovation of Fujian Agriculture and Forestry University under Grant CXZX2016026 and Grant CXZX2016031, and in part by the China ASEAN Maritime Cooperation Fund Project under Grant 2020399.

ABSTRACT In this paper, a hierarchical region merging method is proposed for partitioning synthetic aperture radar (SAR) image into un-overlapping scene area, such as forest regions, urban regions, agricultural regions, and so on. The proposed method mainly consists of two steps: initial over-segmentation and hierarchical regions merging. The over-segmentation uses the watershed transform to the thresholded Bhattacharyya-coefficient-based edge strength map (BESM), and the hierarchical regions merging applies a new region merging cost weighted by a gradually increasing orientated edge strength penalty. There is a defect that the ratio-based edge detector widely used in homogeneous SAR image fails to distinguish the transitions between uniform and texture regions in high spatial resolution SAR image, and yields an initial over-segmentation result with some regions straddling multiple uniform or texture areas. To overcome this, the Bhattacharyya coefficient is used to replace the ratio-based edge detector for extracting the ESM of a SAR image by using a bi-rectangle-window configuration. Multi-scale windows are utilized to capture additional edge information. A new region merging cost is proposed based on the Kuiper's distance, weighted by a new gradually increasing orientated edge strength penalty term. The hierarchical region merging criterion is obtained with the increasing of the strength of the edge penalty. The effectiveness of the proposed method is demonstrated by comparing it qualitatively and quantitatively with several state-of-the-art methods.

INDEX TERMS Synthetic aperture radar (SAR) image segmentation, Bhattacharyya coefficient, hierarchical region merging, Kuiper's distance.

I. INTRODUCTION

Synthetic Aperture Radar (SAR) imaging system is widely used in various applications, such as environment surveillance and change detection of the earth's surface, due to SAR's active microwave imaging mechanism [1]. In SAR-image-based information extraction and scene understanding, SAR image segmentation is considered to be a fundamental problem (e.g., [2], [3]), which provides the structural information of the scene by segmenting its SAR image into several disjoint homogeneous regions. SAR image segmentation becomes more difficult than an optical image segmentation because of the existence of speckle noise produced by coherent imaging principle. One kind of the major SAR image segmentation methods is the approach based on region merging, which is widely used in SAR image segmentation (e.g., [4], [5]) and optical image segmentation (e.g., [6]–[8]).

Starting from an initial partition, the region-merging-based image segmentation method iteratively merges the most similar two adjacent region-pair based on a certain region merging cost and is terminated while the region merging cost of the most similar two adjacent region-pair is greater than a preset

The associate editor coordinating the review of this manuscript and approving it for publication was Bora Onat.

threshold. There are two major factors involved with this kind of method: initial partitioning and region merging. Initial partitioning segments an image into over-segmentation, which is an important step for generating high-quality segmentation results. This is because the pixel set on boundaries in a final segmentation result is a subset of the pixel set on the boundaries of an initial partition. Region merging consists of region merging cost and criterion. A region merging cost determines whether two adjacent regions should be merged into a large region, and a region merging criterion is a procedure to find out the candidate region-pairs that may be merged in the region merging process.

A. INITIAL PARTITIONING

In the community of SAR image segmentation, one of the widely used initial partitioning methods is the watershed transform of the Edge Strength Map (ESM) of a SAR image (e.g., [9]–[14]). The ESM is obtained by using gradient information (e.g., [9], [10]) or the ratio of two means calculated from two set of pixel values delimited by the parallel rectangle bi-window (e.g., [11]–[14]). Due to the existence of the multiplicative speckle noise in SAR images and the constant false alarm rate of the ratio-based detectors (e.g., [15]–[17]), the ratio-based initial partitioning methods outperform the gradient-based ones in SAR images. However, the ratio-based methods may result in the phenomenon that some initial segmented regions straddle multiple homogeneous regions in high resolution SAR images with abundant textures, as only the first-order statistic was used in the ratio-based edge detectors.

B. REGION MERGING

The region merging process is controlled by the region merging cost that is generally designed by exploiting the Statistical Similarity Measurement (SSM) of two adjacent regions and the edge penalty term of a segmentation results. The simple grayscale-statistics-based SSM in SAR images will yield good segmentation for the low-resolution SAR images composed of farmland scenes, but it can possibly result in over-segmentation for high-resolution SAR images with heavy textures [9]. Although some complex distributions can be used to remedy this issue (e.g., [18]–[20]), it may still fail to find accurate segmentation regions because of the mismatch between the adopted distribution and the real distribution of SAR image pixels [21]. The introduction of the edge penalty term in region merging cost can make the boundaries of the segmented regions smoother. The length and the strength information of the common boundaries of two adjacent regions is used to generate the edge penalty term (e.g., [9], [22], [23]), and it is gradually increased during the region merging. This kind of edge penalty has two beneficial functions: 1) reducing influence of the inaccuracy of parameter estimation in the incipient stage of region merging, and 2) producing hierarchical segmentation results with the change of the strength of a penalty term.

In this paper, Bhattacharyya-based ESM (BESM) is presented to replace the above mentioned Ratio-based ESM (RESM) in the watershed based initial partition. This is inspired by the demonstration that the Bhattacharyya coefficient is an efficient candidate for contrast measure in optical images (e.g., [24], [25]) and polarimetric and interferometric SAR images [26]. BESM is generated by calculating the Bhattacharyya coefficient between two statistical histograms of the two pixel sets in two parallel rectangles on opposite sides of the pixel. Multiple direction and scale parallel rectangles are used to capture additional edge information. The region merging cost is produced via weighting the SSM, which is measured by the Kuiper's distance of two adjacent regions, by gradually increasing orientated edge strength penalty term. The main contributions of this paper are summarized as follows: 1) the Bhattacharyya coefficient of two statistical histograms is used to extract ESM of a SAR image, which is competent to detect the transitional area between homogeneous and heterogeneous regions in high resolution SAR images with abundant textures; 2) a novel Gradually Increasing Orientated Edge Strength Penalty (GIOESP) term is presented, effectively exploiting orientated BESM; and 3) a novel region merging cost is designed via combination of the Kuiper's distance and the GIOESP term with the product-type fusion.

This paper is organized as follows: We briefly survey the closely related literature in Section II. Section III reviews the definition of the SAR image segmentation and describes the outline of the proposed method. The initial partition method based on the Bhattacharyya coefficient is proposed in Section IV and, moreover, its characteristics are analyzed through comparison with the ratio-based initial partition. In Section V, a hierarchical region merging process with the GIOESP weighted Kuiper's distance is presented. Section VI reports the experimental results on synthetic and real SAR images. The proposed method is qualitatively and quantitatively evaluated in comparison to several state-of-the-art methods. Finally, we conclude this paper in Section VII.

II. RELATED WORK

In this section, we survey the related work about initial over-segmentation methods for SAR images in Section II-A as well as region-merging-based segmentation methods of SAR images in Section II-B, respectively.

A. INITIAL OVER-SEGMENTATION

A lot of methods have been proposed to generate initial over-segmentation results (or referred to as superpixels) on optical images. The Turbopixels method [27] generated regular and uniform initial over-segmentation results using level-set method driven by a geometric flow under uniformly distributed seeds. The locations of initial seeds and the instability of the level-set method maybe affect the accuracy of boundary localization of this method. Based on the K-means clustering with limited searching space, SLIC [28]

has efficient performance; however, an auxiliary operation has to be taken to ensure that the produced initial partition regions are connected. Graph-cut [29] and N-cuts [30] generate regular and compact over-segmentation results using graph-based methods, but which result in higher time and space complexity. Entropy-based algorithm [31] generates over-segmentation results with regular size, but with higher time complexity yet. Because of parallel implementation of watershed transforming [32], watershed-based algorithms generate over-segmentation results efficiently, whose adherence to image boundaries depend on the accuracy of the ESM extracted from initial images.

Generally, the gradient-based and the ratio-based methods are two approaches to generate ESM in SAR images, e.g., [9], [13] and [16]. This has been discussed, in [13], that the ratio-based method outperforms the gradient-based one in SAR images. In [14], we improved the ratio-based approach to compute ratio of averages through rotating bi-windows for initial over-segmentation of low-resolution SAR images. But this improved method yet fails to find out boundaries between homogeneous area and texture area, and thus results in under-segmentation regions around transition areas between different kinds of texture areas. Utilizing coefficient of variation (CV) as a measurement of homogeneity of a region, literature [33] proposed a region-growing-based initial over-segmentation method starting from an initial seed set. Because of mandatory operation for incorporating an un-labeled single pixel into the adjacent region with the lowest CV and inaccuracy of CV estimated from a small region, this method produced initial segmentation region with imprecise edge location and under-segmentation. Employing finite mixture models, literature [34] generated initial over-segmentation with low under-segmentation error, however, whose accuracy of edge localization and compactness of image regions suffered from inaccurate estimation of parameters of statistical models.

B. HIERARCHICAL REGION MERGING

Region merging process involves similarity measurement of two adjacent regions, order of merging regions and generation of final segmentation results (or termination criterion). Based on statistical modeling of images data and special region merging order, SRM [35] generated good segmentation results, but its performance depended on the designed merging order in a large part. Using the region adjacency graph (RAG) representation of initial segmented region generated by operating watershed transform on gradient magnitude, literature [36] presented a fast greedy region merging algorithm with a small research space in the nearest neighbor graph of the RAG. In [37], a set of information theory based hierarchical region merging algorithms were proposed by using a statistical partition selection criterion to obtain final segmentation results.

For the community of SAR image segmentation, image regions are usually described by using parameter or non-parameter statistical model to deal with speckle noise produced by imaging system. Based on the statistical model, the similarity or dissimilarity between adjacent regions is designed. A region-based hierarchical Markov random field (MRF) model was proposed for generation of multi-resolution segmentation, in [38], and Gamma distribution was used to describe image regions, which limited this method into segmentation of homogeneous low-resolution SAR image. In order to cope with the influence of speckle in SAR images, literature [5] employed the generalized gamma distribution for modeling SAR image regions and a MRF model was used to carry out region merging, however its method generating initial segmentation results may result in the regions with serration boundaries.

Recently, the hierarchies of image segmentation have been studied in the viewpoint of the representation and the performance of hierarchical partition. In [39], authors studied three methods to describe hierarchies of segmentation, saliency maps, minimum spanning trees and ques flat zones, as well as their equivalence. And, in [40], an evaluation framework was proposed to measure the hierarchies of watershed-based segmentation in the phase of edge localization and object detection.

III. DEFINITION OF SEGMENTATION AND FRAMEWORK OF THE PROPOSED METHOD

Let $\Omega = \{(x, y) : x \in \{1, 2, \ldots, N_x\}, y \in \{1, 2, \ldots, N_y\}\}$ denote the discrete 2-D rectangular grid, where N_x and N_y are the numbers of the rows and the columns of the grid, respectively. A SAR image is defined as $I(x, y) : \Omega \to \mathbb{R}$, where $\mathbb{R}$ is the real set. A segmentation $\Re$ of a SAR image is to segment it into several disjoint regions, $\Omega_k \subseteq \Omega, k = 1, 2, \ldots, K$, in which every region is delimited by a closed and single pixel wide contour, $\partial\Omega_k, k = 1, 2, \ldots, K$, and is homogeneous with respect to a given criterion. The segmentation $\Re = \{\Omega_k, k = 1, 2, \ldots, K\}$ and the corresponding contour $\partial\Re = \{\partial\Omega_k, k = 1, 2, \ldots, K\}$ satisfy [9]:

$$\begin{aligned}
&(i) \cup_{k=1}^{K} \Omega_k \cup_{k=1}^{K} \partial\Omega_k = \Omega \\
&(ii) \forall i \neq j, \Omega_i \cap \Omega_j = \emptyset \\
&(iii) \forall i, j, \Omega_i \cap \partial\Omega_j = \emptyset \\
&(iv) \partial\Omega_i \cap \partial\Omega_j \neq \emptyset \text{ if regions } \Omega_i \text{ and } \Omega_j \text{ are adjacent}.
\end{aligned} \tag{1}$$

(i) implies that any pixel in an image belongs either to a region or to a boundary, (ii) indicates that the segmented regions are mutually disjointed, and (iii) illustrates that the pixels belonging to any closed one-pixel boundary are not part of any region. If two regions Ω_i and Ω_j are adjacent, then their shared common boundary is $\partial\Omega_i \cap \partial\Omega_j$ just as shown in (iv).

The Region Adjacent Graph (RAG) [36] is a convenient way to represent image segmentation results. RAG is an undirected graph denoted by RAG(V, E, W). The node set $V = \{v_k, k = 1, 2, \ldots, K\}$ indicates K regions in the segmentation results. The edge set E is a subset of $V \times V$. If regions Ω_k and Ω_p are adjacent, then $e_m = (v_k, v_p) \in E$ exists in the edge set E. The W is a $|V|$ by $|V|$ weight matrix, where,

if $e_m = (v_k, v_p) \in E$, then $W(v_k, v_p)$ and $W(v_p, v_k)$ are assigned region merging costs (computed by expression (9) in Section V-C) of two adjacent regions Ω_k and Ω_p, otherwise they are assigned an infinite.

The framework of the proposed SAR image segmentation method consists of the initial segmentation and the hierarchical region merging, as shown in Fig. 1. the initial segmentation results can be attained via watershed transform of the thresholded Multi-scale BESM (MBESM). Starting from the initial partition, the most similar adjacent region-pair is iteratively merged by employing the new region merging cost that is designed by using the Kuiper's distance of an adjacent region-pair that is weighted by a Gradually Increasing Orientated Edge Strength Penalty (GIOESP) term.

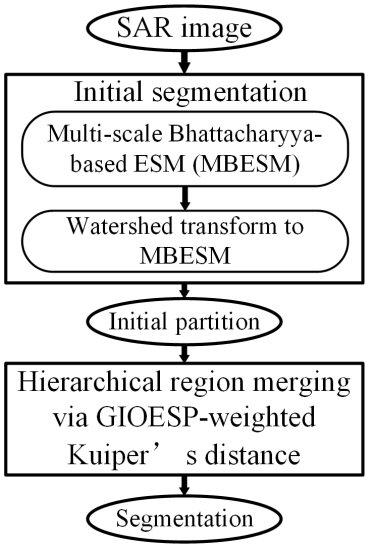

FIGURE 1. The framework of the proposed method.

IV. INITIAL PARTITION USING BHATTACHARYYA COEFFICIENT

Since the process of region merging iteratively merges the two most similar adjacent regions into a large region starting from an initial partition, and the positions of the boundaries of regions cannot be adjusted during this procedure, it is desired that an initial partition satisfies the following property:

$$\forall \Omega_i \in \Re_{ini}, \quad \exists R_j \in \Re_{opt} : \Omega_i \subseteq R_j. \tag{2}$$

where, $\Re_{ini}$ and $\Re_{opt}$ indicate the initial and the optimal segmentations, respectively. Expression (2) indicates that any region in the initial partition is composed of the pixels that belong to a common homogeneous region in the optimal segmentation and the edges that need to be detected in the optimal segmentation must be labeled in the initial partition.

Different from the Statistical Region Growing (SRG) [33] and the RESM-based watershed transform [14] initial partition methods, in this paper, the Bhattacharyya Coefficient (BHC) of the two empirical distribution functions estimated by using pixels in a multi-scale rotatable rectangle bi-window is used to calculate the ESM of an original SAR image. The obtained ESM is named Multi-scale Bhattacharyya-based ESM (MBESM). Then, the initial partition is generated via watershed transform on the thresholded MBESM.

The BHC of a SAR image $I(x, y)$ is calculated based on the quantified version of the original SAR image. That is to say, we first quantify a SAR image data on a finite number of Q values, and the quantified image is $I_q(x, y) : \Omega \rightarrow \{1, 2, \ldots, Q\}$. The quantization scheme used here consists of a histogram equalization of the original SAR image and reassignment of the level of the equalized image. Firstly, a histogram equalization of the original SAR image is performed, which defined by $s_k = \sum_{j=1}^{k} h(j)$, where $h(k)$ is the proportion of gray level k in the original SAR image. Here $k \in \{1, 2, \ldots, L\}$ and $s_k \in [0, 1]$ are gray levels in the original SAR image and the equalized level, respectively. We can then obtain the quantified image $I_q(x, y)$, $I_p(x, y) = p$, if $s_{I(x,y)} \in [(p-1)/Q\ ,\ p/Q]$, else $I_q(x, y) = Q$.

Based on the quantified image $I_q(x, y)$, an orientated BHC, $BHC(x, y, \theta)$, of a SAR image is computed using a rotatable parallel rectangle bi-window, as shown in Fig. 2(a). At the center of a pixel point (x, y), two histograms are calculated from two sets of quantified intensity values in $I_q(x, y)$ covered by these two parallel rectangle widows, as shown in Fig. 2(c). The obtained two histograms are noted by $h_u(n)$ and $h_l(n)$, $n = 1, 2, \ldots, Q$, respectively (see Fig. 2(d)), and the orientated BHC, $BHC(x, y, \theta)$, at point (x, y) is calculated by

$$BHC\ (x, y, \theta) = -\ln\left[\sum_{k=1}^{Q} \left(h_u\ (k) \cdot h_l\ (k)\right)^{1/2}\right] \tag{3}$$

angle θ is uniformly sampled in the interval $[0\ ,\ \pi]$ in the computation. Eight orientations are used in all our applications. Then, the second-order Savitzky-Golay filtering [41] is used to enhance local maxima and smooth out false peaks in the direction orthogonal to θ in $BHC(x, y, \theta)$. Figs. 2(b)-(e) show an example of a computation of an oriented BHC of a SAR image. In Fig. 2(e), a strong oriented BHC means that the corresponding pixel point is likely to lie on the boundary between two distinct regions.

For a given SAR image, to detect trivial as well as some important edge information of the SAR image, three BHCs, $BHC_s(x, y, \theta), s = W_1, W_2, W_3$, are calculated at three scales: $[W_1 = \{l/2, w/2, d, \theta, (x, y)\}, W_2 = \{l, w, d, \theta, (x, y)\}$, and $W_3 = \{2l, 2w, d, \theta, (x, y)\}]$. One then obtains the final oriented BHC of the SAR image by linearly combining the three BHCs:

$$BHC\ (x, y, \theta) = \sum_{s \in \{W_1, W_2, W_3\}} \alpha_s \cdot BHC_s\ (x, y, \theta) \tag{4}$$

where s indicates scales, and the parameters α_s represent the prior knowledge about the three BHCs with different scales. There are more trivial details resulted from the speckle noise in the BHC obtained by using the small scale W_1, and, by comparison, more important information about the

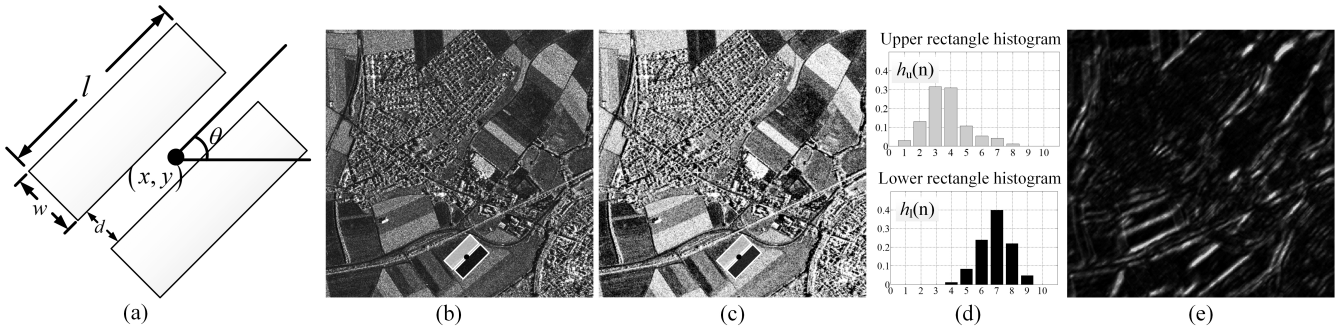

FIGURE 2. Oriented Bhattacharyya coefficient (BHC) of two histograms. (a) shows a rotatable parallel rectangle bi-window $W = \{l, w, d, \theta, b(x, y)\}$ at a center pixel point (x, y). (b) gives an intensity-format SAR image, in which a parallel rectangle bi-window centered at a center pixel, represented by a black solid circle, and rotated through θ angle around on this center pixel exists. A quantified version of the SAR image in (b) is shown in (c), where the quantitative level Q is *10*. This quantified image is used to calculate the BHC of the original SAR image. In (d), the gray and the black distributions are the histograms of the quantified intensity in the gray and the black rectangle windows in (c), respectively. (e) shows the BHCs of the original SAR image shown in (b) that are calculated by using each pixel along the orientated angle $\pi/4$, where the length and the width of each rectangle window are *9* and *4* pixels, respectively, and the space between these two rectangles is a single pixel. Note that (b) displays an amplitude-format SAR image for an illustrative purpose.

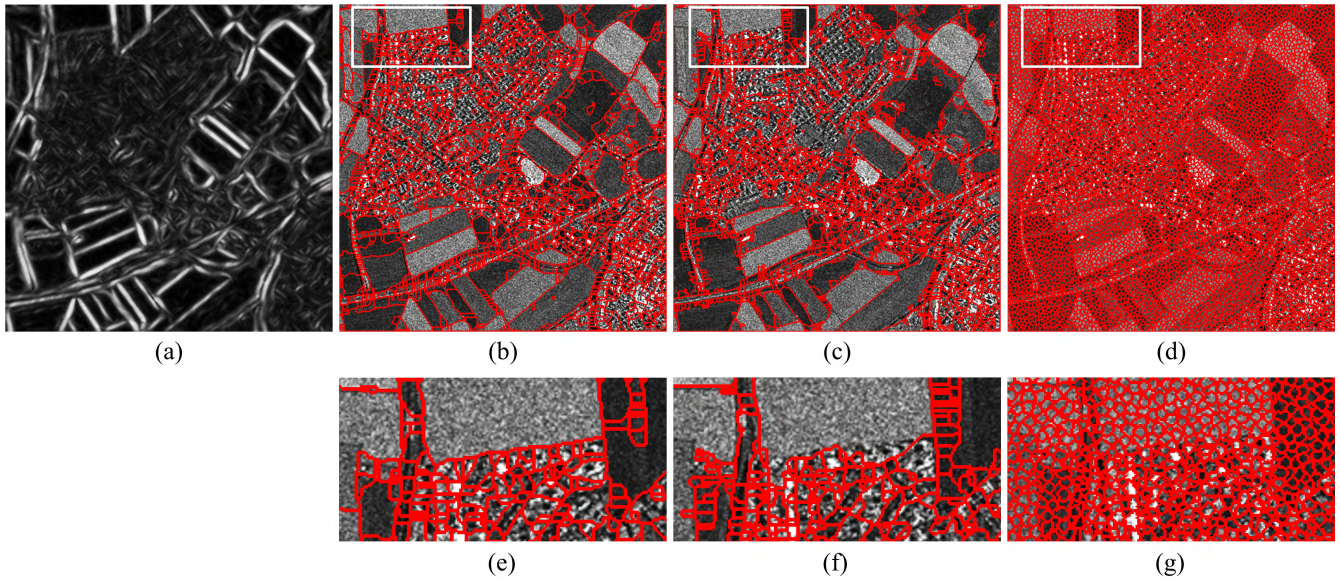

FIGURE 3. Comparisons of initial partition results produced by the proposed BHC-based watershed transform, the RESM-based watershed transform [14] and the SRG [33]. (a) The thresholded BHC of the quantified image in Fig. 2(c) calculated by using three bi-windows configures: $W_1 = \{11, 4, 1, \theta = \{0, \pi/8, \ldots, (7\pi)/8\}\}$, $W_2 = \{21, 8, 1, \theta = \{0, \pi/8, \ldots, (7\pi)/8\}\}$, and $W_3 = \{41, 16, 1, \theta = \{0, \pi/8, \ldots, (7\pi)/8\}\}$. (b) Initial partition result by the proposed BHC-based watershed transform. (c) Initial partition result by the RESM-based watershed transform [14]. (d) Initial partition result by the SRG [33]. (e) [respectively, (f) and (g)] Zoom of a local rectangle area extracted from (b) [respectively, (c) and (d)].

boundaries of an original SAR image exists in the BHC produced by utilizing the large scale W_3. Taking the maximum response over orientations produces our ESM at each location:

$$BHC\,(x, y) = \max_{\theta \in [0,\pi]} \{BHC\,(x, y, \theta)\} \tag{5}$$

It is well known that the number of regions generated by using the watershed transform [32] on an ESM is determined by the number of local minima in the ESM. A mass of local minima in an ESM lead to fragmentized regions, which will be alleviated by a simple α percentile-based thresholding operation of the ESM, as was done in [14]. Here, the same thresholding operation is done on the BHC, $BHC(x, y)$, to produce a thresholded BHC and then the initial partition of the SAR image is generated utilizing watershed transform on the thresholded BHC.

Fig. 3 shows the thresholded BHC of the SAR image in Fig. 2(c), as well as the initial partition results obtained by the BHC-based watershed transform, the RESM-based watershed transform [14], the SRG [33], and their zooms of local rectangle areas. The initial partition results in Fig. 3(b), (c) and (d) consist of 2089, 2750, and 8289 regions, respectively. Moreover, the most of edges in the SAR image are detected and precisely located by the proposed BHC-based method. However, some important edges in

the SAR image cannot be detected by the RESM-based method and the SRG method precisely. The SRG method also generates more fragmentized regions than the other two methods.

V. HIERARCHICAL REGION MERGING WITH GIOESP WEIGHTED KUIPER'S DISTANCE

The goal of a region merging is merging adjacent regions starting from an initial partition to generate the final segmentation results, which is executed by iteratively merging the most similar adjacent region-pairs under the control of a region merging cost. The order of merging adjacent region-pairs in a region merging process and the quality of final segmentation results are determined by the region merging cost. In this section, the Statistical Similarity Measure (SSM) based on the Kuiper's distance [42] between two histograms calculated from the two adjacent regions is proposed to measure the similarity of two adjacent regions. In order to restrict the effect caused by inaccuracy of estimated histograms of two adjacent regions on final segmentation results, a Gradually Increasing Orientated Edge Strength Penalty (GIOESP) using Orientated Bhattacharyya Coefficient (OBHC) is proposed to weight the Kuiper's distance of two adjacent regions.

A. SSM OF TWO REGIONS USING KUIPER'S DISTANCE

An SSM is used to judge whether two pixel-value sets in two adjacent regions are drawn from the identical probability distribution. In the community of SAR image processing, the SSM between two adjacent regions is designed based on the hypothesis that the pixel-value sets in regions obey a certain probability distribution, such as Gamma distribution [5], G^0 distribution [18], and so on. The main problem with these methods is with the parameters' estimation of these distributions and the model mismatch between the adopted distribution model and the SAR image data. The Kuiper's distance between two histograms estimated from two adjacent regions is used to determine whether the two adjacent regions are drawn from an identical probability distribution model.

Let $\Omega_1, \Omega_2 \in \Re_K$ be two adjacent regions in a segmentation with K regions, and $h_1(k)$ and $h_2(k)$, $k = 1, 2, \ldots, Q$, are histograms, with Q bins, of regions Ω_1 and Ω_2, respectively. They are calculated by using the quantified image $I_q(x, y)$ of original SAR image $I(x, y)$ with quantization level Q. The standard K-S distance [42] is used to measure the difference between $h_1(k)$ and $h_2(k)$, which is defined as the maximum value of the absolute difference between two cumulative distribution functions $S_1(k)$ and $S_2(k), k = 1, 2, \ldots, Q$. These two cumulative functions are respectively calculated from the two histograms $h_1(k)$ and $h_2(k)$, $S_i(k) = \sum_{j=1}^{k} h_i(j)$, $i = 1, 2$. It has been shown [42] that the standard K-S distance can effectively measure the difference between two cumulative distribution functions when the maximum value of the absolute difference between these two cumulative distribution functions occurs around the median values of these two calculated histograms. However, this measurement may be failed if the maximum value happens at the tails of these two distribution function. The Kuiper's distance [42] is introduced to measure the similarity of two adjacent regions in this paper, which is a variant of the standard K-S distance mentioned above, to improve the performance of the standard K-S distance. The Kuiper's distance between two cumulative distribution functions is defined as [42]

$$V(\Omega_1, \Omega_2) = \max_{k=1,2,\cdots,Q} (S_1(k) - S_2(k)) + \max_{k=1,2,\cdots,Q} (S_2(k) - S_1(k)). \quad (6)$$

As the same technique used in [42], considering the influence of the areas of two adjacent regions on the statistical measure V, an area-weighted Kuiper's distance D is used to measure the similarity of the two adjacent regions [43]:

$$D(\Omega_1, \Omega_2) = (\sqrt{N_e} + 0.155 + \frac{0.24}{\sqrt{N_e}}) V(\Omega_1, \Omega_2). \quad (7)$$

where $N_e = N_1 \times N_2/(N_1 + N_2)$, and N_1 and N_2 are areas of the two adjacent regions, respectively. A large value of D means a greater dissimilarity between the two regions.

In this paper, replacing the standard K-S distance with the Kuiper's distance makes the best of the sensitivity of the Kuiper's distance at the tails of two probability distributions [42] to measure the similarity of two adjacent regions. It is a fact that the pixel values in a high-resolution SAR image obey a heavy-tailed probability distribution. This property coincides with the sensitivity of the Kuiper's distance, so it is convinced that the Kuiper's distance is more effective in measuring similarity of two adjacent regions in a high-resolution SAR image than the standard K-S distance.

B. GIOESP-WEIGHTED REGION MERGING COST

It has been shown [4], [5], [9], [18] that the penalty or the regularization mechanism plays an important role in obtaining meaningful segmentation results. The mechanism is implemented by introducing prior information of a segmentation result into a region merging cost, which generally involves the length of boundaries, the area of each region, or both. The goal of the penalty term in a region merging cost is to produce the final segmentation results possessing some desired properties, such as smoother, bigger and fewer regions and boundaries. In practice, the limitations of the final segmentation results mentioned above are necessary, since there are a lot of fragmentized regions and rough boundaries in the segmentation results, which are resulted from noise and textures in an image. Due to existence of strong speckle noise in a SAR image, this is even more severe in a SAR image segmentation.

In this paper, a Gradually Increasing Orientated Edge Strength Penalty (GIOESP) of a common boundary between two adjacent regions is proposed based on the oriented BHC (OBHC) and length of the common boundary.

The GIOESP, $w(\Omega_1, \Omega_2)$, is defined as

$$w(\Omega_1, \Omega_2) = \frac{1}{|\Gamma_{1,2}|} L,$$
$$L = \sum_{(x,y)\in\Gamma_{1,2}} \left(1 - \exp\left\{-\frac{\left(OBHC\left(x, y, \theta_{(x,y)}\right)\right)^2}{K^2}\right\}\right). \quad (8)$$

where $\Gamma_{1,2}$ is a set of pixel coordinates on the common boundary between two adjacent regions Ω_1 and Ω_2. $|\Gamma_{1,2}|$ is the cardinality of the set $\Gamma_{1,2}$, i.e., the length of the common boundary $\Gamma_{1,2}$, and $OBHC\left(x, y, \theta_{(x,y)}\right)$ is the oriented BHC of a pixel (x, y) along the direction $\theta_{(x,y)}$ that is estimated by the polygon approximation of the common boundary. K is a parameter which is used to tune the strength of the penalty term, and the strength is in inverse proportion to the parameter K.

C. HIERARCHICAL REGION MERGING CRITERION AND IT'S PROPERTIES

To obtain satisfactory segmentation results, it is necessary to combine the SSM and the GIOESP to form a region merging cost to determine whether two adjacent regions can be merged. The product-type fusion of the SSM and the GIOESP is used to construct region merging cost, as following:

$$\kappa(\Omega_1, \Omega_2) = w(\Omega_1, \Omega_2) \cdot D(\Omega_1, \Omega_2). \quad (9)$$

As shown in Algorithm (1), a hierarchical region merging criterion is proposed based on the region merging cost $\kappa(\Omega_1, \Omega_2)$.

The proposed region merging criterion, (i.e., Algorithm 1), starts from an initial partition and its RAG expression. The hierarchical segmentation results are obtained by gradually increasing of parameter K. The region merging process is terminated when all pixels in the image are segmented into one region. There are two parameters, α and T_{merg}, needed to be set, which respectively affect the number of levels and the number of the region of each level in the outputted hierarchical segmentation tree. The smaller α is, the greater the number of levels there are in the hierarchical segmentation tree, and the number of regions in each level of the segmentation tree is in direct proportion to the parameter T_{merg}.

Observe that the output of the Algorithm 1 is a tree, which is composed of hierarchical segmentation results and whose leaf nodes consist of the finest segmentation regions and root node is the image itself. Fig. 4 shows an example of a hierarchical segmentation tree of a synthetic SAR image. From the Fig. 4, we can see that the expression of the hierarchical segmentation tree gives one a chance to choose the segmentation regions to satisfy different applications.

Algorithm 1 Hierarchical Region Merging Criterion

Input: Initial segmentation results $\Re_{ini}$ by the MBESM-based watershed transform of a SAR image.

Output: Hierarchical region merging results shown by a tree.

1: Initialize $i = 0$ and $K = 0.01$ in Eq. 8
2: Initialize the RAG, RAG(V_i, E_i, W_i), of the initial partition results $\Re_{ini}$ using the region merging cost, Eq. 9, to compute edgeąŕs weight of the RAG
3: **while** the number of nodes in RAG(V_i, E_i, W_i) is greater than one and $K < 2$
4: Find the minimal edge $e_{\min}$ from the RAG(V_i, E_i, W_i)
5: **while** the weight $w(e_{\min})$ is not greater than the threshold T_{merg}
6: Merge two nodes, $v_{\min\_1}$ and $v_{\min\_2}$, connected by the edge $e_{\min}$
7: Update the weight of the edges connected to node $v_{\min\_1}$ or $v_{\min\_2}$ in the RAG(V_i, E_i, W_i) using Eq. 9
8: Find the minimal edge $e_{\min}$ from the RAG (V_i, E_i, W_i)
9: **end while**
10: Update $K = K + \alpha$, save the RAG(V_i, E_i, W_i) into the ith level of hierarchical tree, $V_{i+1} = V_i, E_{i+1} = E_i, W_{i+1} = W_i$, and $i = i + 1$.
11: Recalculate the weights of all edges in the RAG(V_i, E_i, W_i) using region merging cost, Eq. 9 with the updated parameter K
12: **end while**
13: **return** the hierarchical tree of the segmentation results.

VI. EXPERIMENTAL RESULTS AND PERFORMANCE EVALUATION

This section shows the experimental results of the proposed method for synthetic and real SAR images. In addition, the method is compared with several state-of-the-art methods, i.e., MDL [4], RCBLP [14], IRGS [9], and CHUMSIS [44]. The Precision-Recall (P-R) framework [45] is used to quantitatively evaluate and compare the performance of different segmentation methods for the boundary quality, as well as the segment covering criteria, the Probabilistic Rand index and the Variation of Information [45] are introduced for the assessment of the region quality of segmentation results.

The proposed segmentation method includes several adjustable parameters. The values of these parameters are selected from a mass of experiments as their default setting used for all segmentation experiments in this paper. The quantitative level Q in the computation both of the BHC for initial partition and the Kuiper's distance of region merging is set to 10 for balancing between the robustness for speckle noise and the detection of different texture features in a SAR image. The bi-window configurations are set with three scales: $W_1 = \{11, 4, 1, \theta = \{0, \pi/8, \ldots, (7\pi)/8\}\}$, $W_2 = \{21, 8, 1, \theta = \{0, \pi/8, \ldots, (7\pi)/8\}\}$, and $W_3 = \{41, 16, 1, \theta = \{0, \pi/8, \ldots, (7\pi)/8\}\}$, to capture more edge information in a SAR image. The weighted sum of these three OBHCs are implemented to generate the BHC, whose weights of the combination are $\alpha_1 = 0.2, \alpha_2 = 0.3$ and $\alpha_3 = 0.5$. The reason why the weights are used to combine the

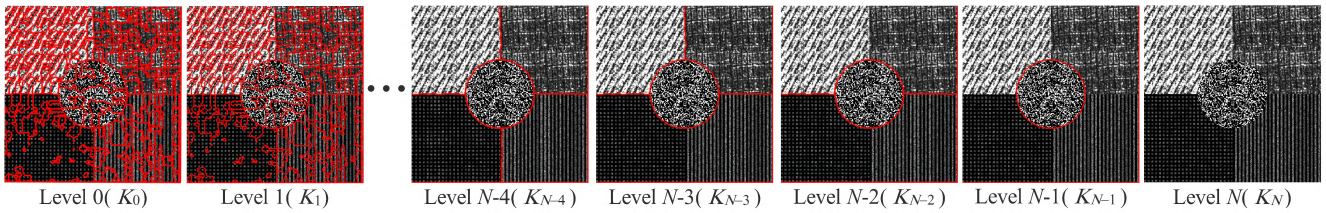

FIGURE 4. Hierarchical tree with $N+1$ hierarchies (or levels) and each one is the segmentation result produced by the Algorithm(1) with a certain parameter K.

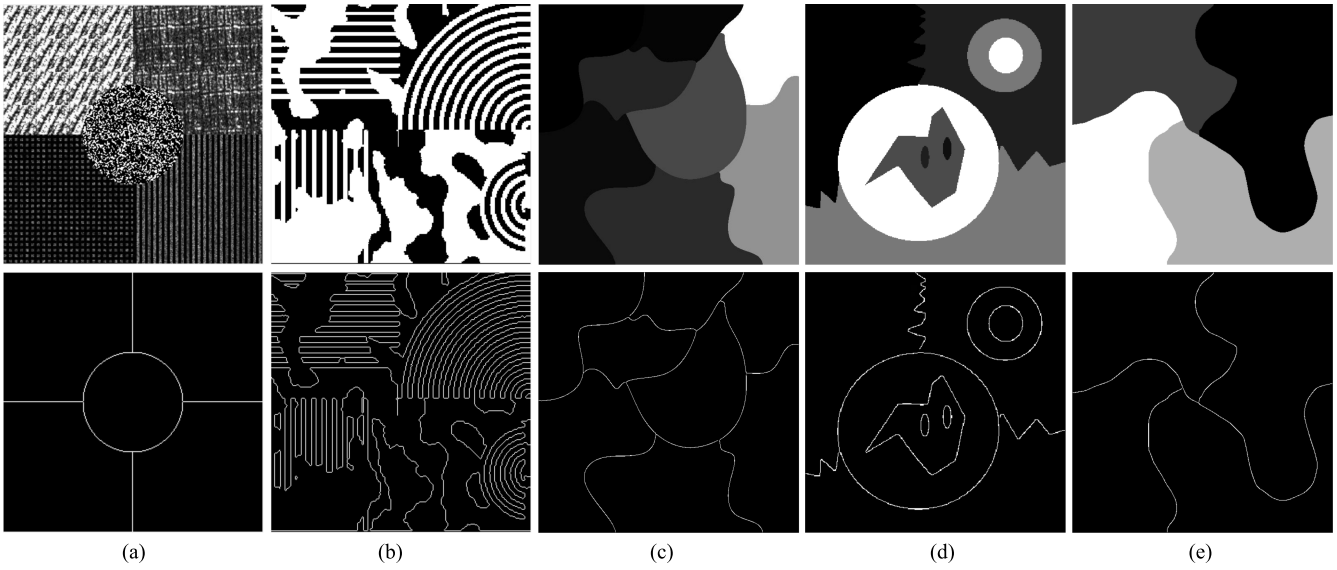

FIGURE 5. Synthetic images and the their Ground Truths (GTs). (a) Synthetic image (S1) tessellated by different regions extracted from real SAR images and its GT. (b)-(e) cartoon images (C1, C2, C3 and C4) tessellated by several disjoint regions with constant reflectance and their GTs, respectively.

OBHCs to produce the HBC is that the OHBC generated by using smaller scale W_1 includes more trivial details resulted from speckle in a SAR image and one produced by utilizing larger scale W_3 possesses more important information about boundaries in a SAR image because of noise suppression of large bi-window. The region merging threshold T_{merg} and the step α of the increasing parameter K in Algorithm(1) are set to 1.0 and 0.001, respectively.

A. SYNTHETIC SAR IMAGE SEGMENTATION

Five synthetic SAR images are used in this paper to evaluate the localization accuracy of boundaries and the region quality of different methods quantitatively. The synthetic SAR image (S1) in Fig. 5(a) is tessellated by five texture regions extracted from different real SAR images and the others, shown in Fig. 5(b)-(e), are cartoon images tessellated by several disjoint regions with constant reflectance. Based on these four cartoon images (C1,C2,C3 and C4), some simulated SAR images with different numbers of looks are generated via the fully developed speckle model. The Ground Truths (GTs) of these five synthetic images are shown in Fig. 5(a)-(e)(bottom row), respectively.

Fig. 6 shows segmentation results produced by different methods on synthetic SAR image S1 and simulated SAR images generated by cartoon image C1 with different numbers of looks. Observe that, from the experimental results

TABLE 1. The number of regions produced by different methods for cartoon scene C1 with different numbers of looks.

	CHUMSIS	MDL	IRGS	RCBLP	proposed
C1(1)	256	73	139	118	**48**
C1(2)	224	128	75	110	**48**
C1(4)	125	141	73	105	**61**

Notes: C1(1), C1(2) and C1(4) indicate 1-look, 2-look and 4-look synthetic SAR image generated by fully developed speckle model with cartoon image C1, respectively.

on the synthetic SAR image S1(see top row in Fig. 6), our proposed method fully gives correct segmentation results along with precision location of boundaries. However, all the other four comparing methods do not fully produce correct segmentation results and generate boundaries with imprecise location resulted from the existence of abundant texture information in S1. With respect to the experimental results shown in Fig. 6 (the second row to bottom row) of simulated SAR images generated by cartoon scene C1 with different numbers of looks, it can be seen that these five methods can detect the most boundaries of the foreground region but suffer from over-segmentation in different degrees. The number of regions of the foreground scene with different numbers of looks is shown in Table 1. It is noticed that the proposed method produces the fewest regions. For the single-look case in the second row shown in Fig. 6, as the speckle noise strengthens, the MDL method does not detect all of

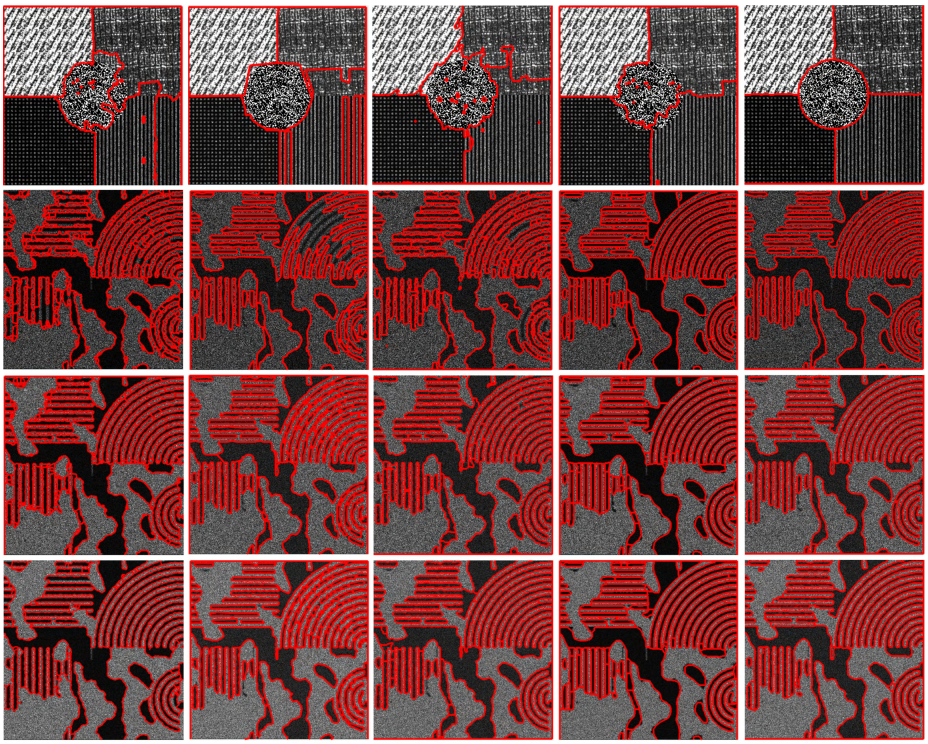

FIGURE 6. Segmentation results of synthetic SAR image S1(top row) and simulated SAR images(from second to bottom row) generated by cartoon image C1 with different numbers of looks (single-look, two-look and four-look, respectively). (a)CHUMSIS [44] (b) MDL [4] (c) IRGS [9] (d) RCBLP [14] (e) proposed.

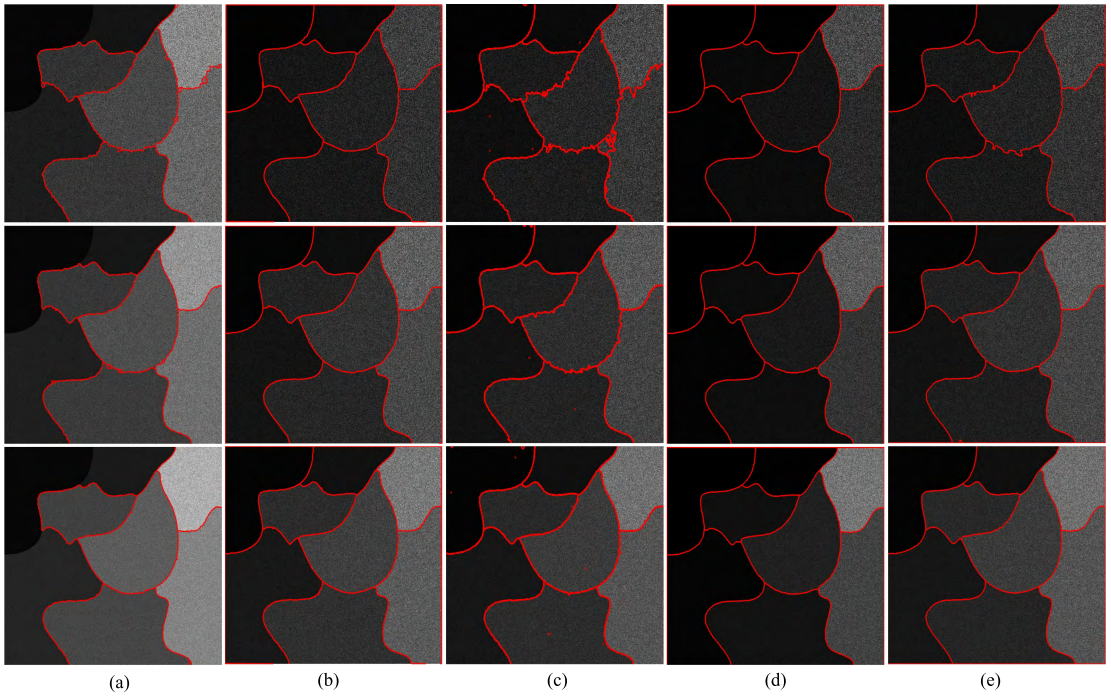

FIGURE 7. Segmentation results of simulated SAR images(from top to bottom row) generated by cartoon image C2 with different numbers of looks (single-look, two-look and four-look, respectively). (a) CHUMSIS [44] (b) MDL [4] (c) IRGS [9] (d) RCBLP [14] (e) proposed.

the foreground regions, and the CHUMSIS and the IRGS methods tend to produce coarse boundaries. The RCBLP and the proposed methods can detect most of foreground regions with the precision location of boundaries and somewhat over-segmentation. In contrast, the proposed method yields fewer regions.

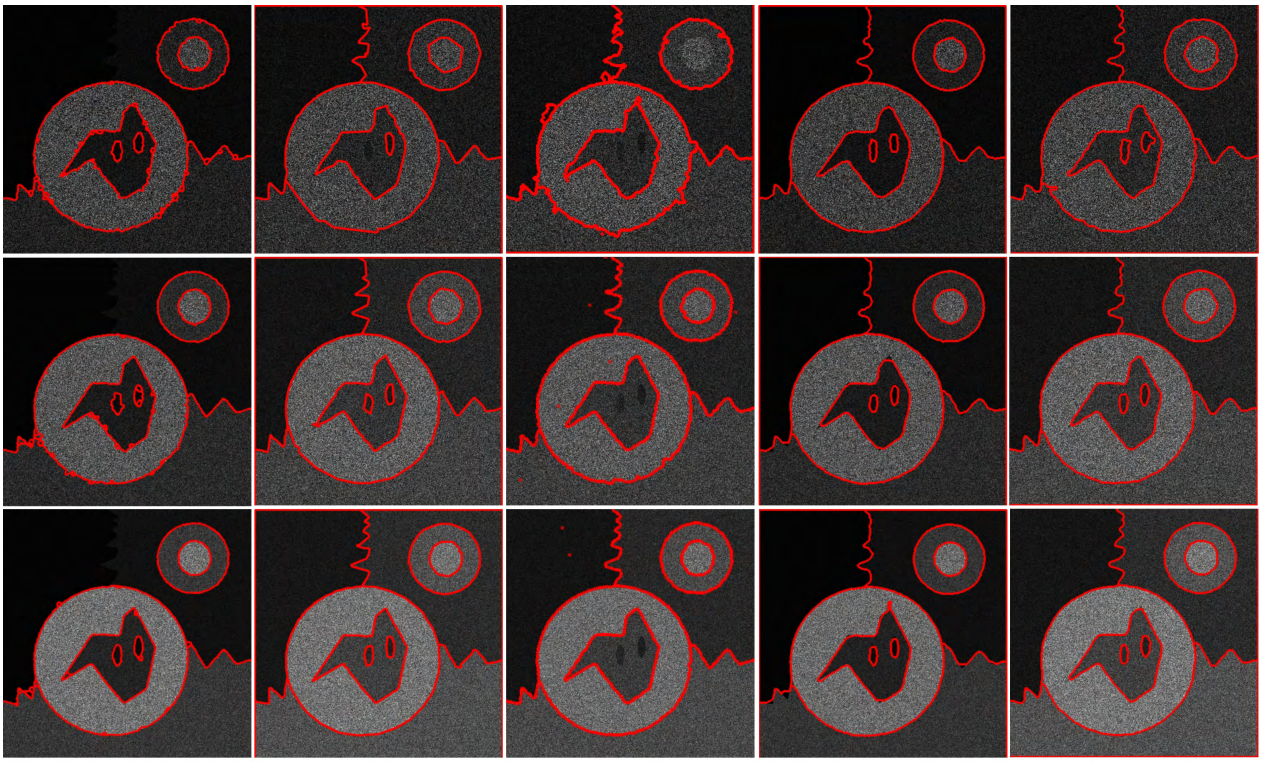

FIGURE 8. Segmentation results of simulated SAR images(from top to bottom row) generated by cartoon image C3 with different numbers of looks (single-look, two-look and four-look, respectively). (a) CHUMSIS [44] (b) MDL [4] (c) IRGS [9] (d) RCBLP [14] (e) proposed.

Fig. 7 to Fig. 9 display segmentation results produced by different approaches on three groups of simulated SAR images generated by three cartoon images, C2, C3 and C4, respectively, with different numbers of looks, single-look, two-look and four-look from top to bottom row in each figure. When it comes to the segmentation results produced by the MDL, the RCBLP and the proposed methods on two-look and four-look simulated SAR images, which are shown from the second to bottom row in each figure of Fig. 7 to Fig. 9, it is not obvious to chose the best one visually. However, comparing with the CHUMSIS and the IRGS methods, these three methods produce high quality results with the high precision location of boundaries and without under-segmentation. In terms of single-look simulated SAR images, as the existence of the strong speckle noise, all of these five methods tend to generate the segmentation results whose boundaries locate in incorrect position. By comparison, the RCBLP method does better than others. Our proposed method outperforms the CHUMSIS and the IRGS methods and is comparable to the MDL method. It is worth noticed that, different from the MDL, the RCBLP and the IRGS methods, the proposed method does not suppose that the SAR images processed obey a certain statistical model.

B. REAL SAR IMAGE SEGMENTATION

In this section, six different real scenes (RS1, RS2, RS3, RS4, RS5 and RS6), which are shown in the first column in Fig. 10 and including agriculture, forest, urban and so on, are utilized to testify the effectiveness of the five methods. The experimental results displayed in Fig. 11 indicate that all the five methods are competent in segmenting homogeneous regions that are tessellated by agricultural scenes. However, comparing to the proposed method, all the other comparing methods fail in the detection of the boundaries between homogeneous and texture regions and give obviously over-segmentation in urban area(see the fifth and sixth rows in Fig. 11). Because the urban areas shown in the fifth and sixth rows in Fig. 11 disobey the piecewise constant cartoon model that the MDL and the RCBLP methods demand, these two methods result in obviously over-segmentation and disappearance of boundaries between agriculture and urban areas. The segmentation results by the CHUMSIS and the IRGS methods show the same characteristics as the MDL and RCBLP methods, over-segmentation in urban areas and failure of detecting boundaries of urban areas. Visually, the proposed method gives better results for urban and forest areas, which benefits from the novel ESM extracting method and the hierarchical region merging criterion.

C. QUANTITATIVE PERFORMANCE ASSESSMENT

In order to evaluate the precision of boundary location of a segmentation result quantitatively, the Precision-Recall (P-R) framework is used to compare the boundaries detected by an algorithm with the GT, where the Precision (P) is the

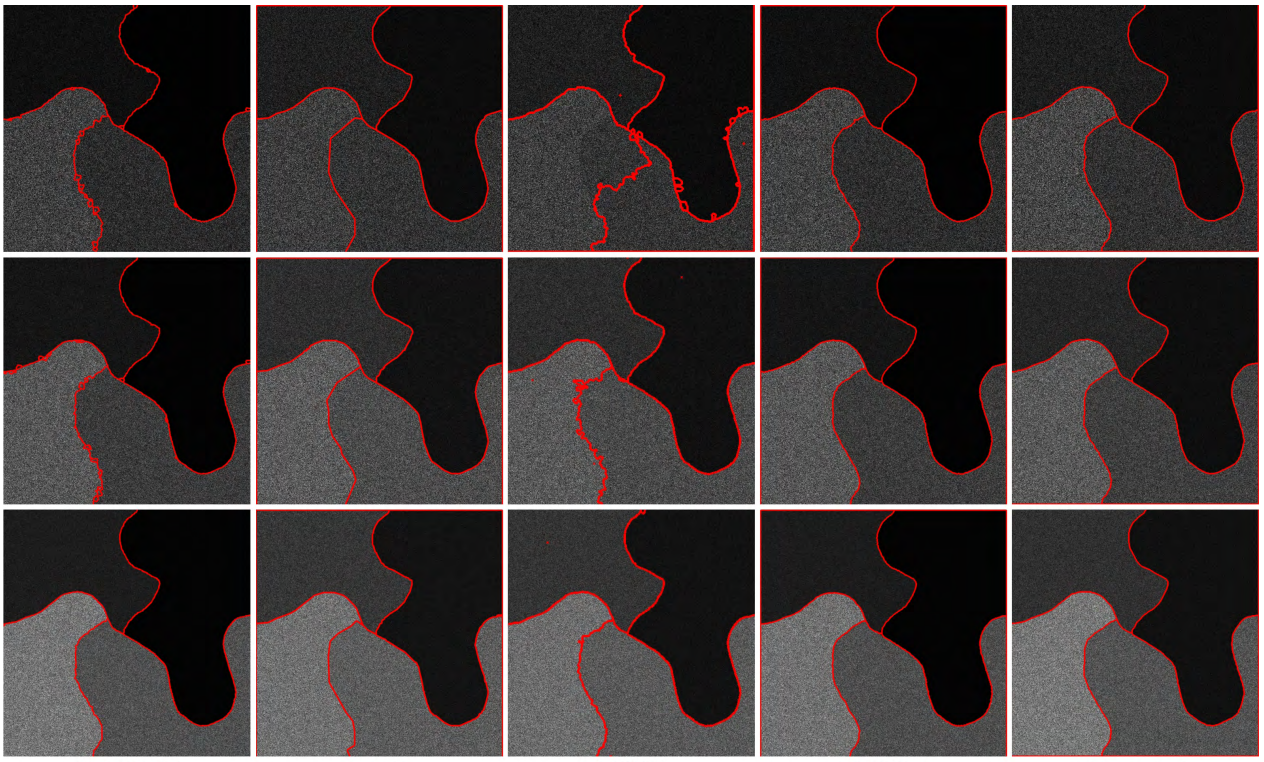

FIGURE 9. Segmentation results of simulated SAR images(from top to bottom row) generated by cartoon image C4 with different numbers of looks (single-look, two-look and four-look, respectively). (a) CHUMSIS [44] (b) MDL [4] (c) IRGS [9] (d) RCBLP [14] (e) proposed.

probability of the edge pixels of segmentation results to be valid and the Recall (R) is the probability of the edge pixels in the GT to be detected. The F-measure is the weighted harmonic mean of R and P [45], which gives an overall boundary quality assessment of a method. A larger F-measure indicates that the edge location of a segmentation result of an image is closer to the GT of the image. A powerful performance descriptor, the P-R curve of a method, will be obtained by changing a parameter of a method if the parameter exist. The ideal segmentation result corresponds to the point (1,1) in the P-R plane, which means that the boundaries of a segmentation result completely match the GT, and the better method produces the P-R curve that is closer to the ideal point (1,1) than ones generated by other methods.

For a set of algorithm segmentation results, related to different hierarchies of a hierarchical algorithm, three quantitative indexes, the segment covering criteria (cov.), the Probabilistic Rand Index (PRI) and the Variation of Information (VI) [45], are used to assess the region quality of the segmentation results with the GT. The cov. and the PRI of a method are equal to one, respectively, indicate that the segmentation result generated by this method fully matches the GT. The closer to one the cov. and the PRI of a method are, the better its performance is. And the VI measures the distance between a set of segmented regions and the GT, so its ideal value is zero.

1) SYNTHETIC AND SIMULATED SAR IMAGES

Fig. 12 plots the P-R curve comparison of the five methods for the synthetic SAR image S1. The recalls, precisions and F-measures of them at the best hierarchy are listed in Table 2. From Fig. 12 and Table 2, it can be seen that the proposed method is superior to the other comparing methods in the boundary quality, which means that the proposed method outperform the other methods in detection of transition between different texture information.

Fig. 13 depicts the P-R curve comparisons of the five methods for the single-look, two-look and four-look simulated SAR images generated by the four cartoon scenes C1,C2,C3 and C4, and their recalls, precisions and F-measures of these images at the best hierarchy are also listed in Table 2. From Fig. 13, it is obvious that, for multi-look simulated SAR images generated by piecewise constant cartoon scenes C1, the five methods obtain similar P-R curve, but, for single-look SAR image, the CHUMSIS method produces lower P-R value than the other methods. However, from Table 2, the proposed method also achieves slightly higher F-measure than the other methods, and, Table 1 indicates that the proposed method produces the segmentation results with the fewest regions, which means that the proposed method gets the minimum over-segmentation in the five methods. For cartoon scenes C2,C3 and C4, Fig. 13 and Table 2 illustrate that the MDL and the RCBLP methods

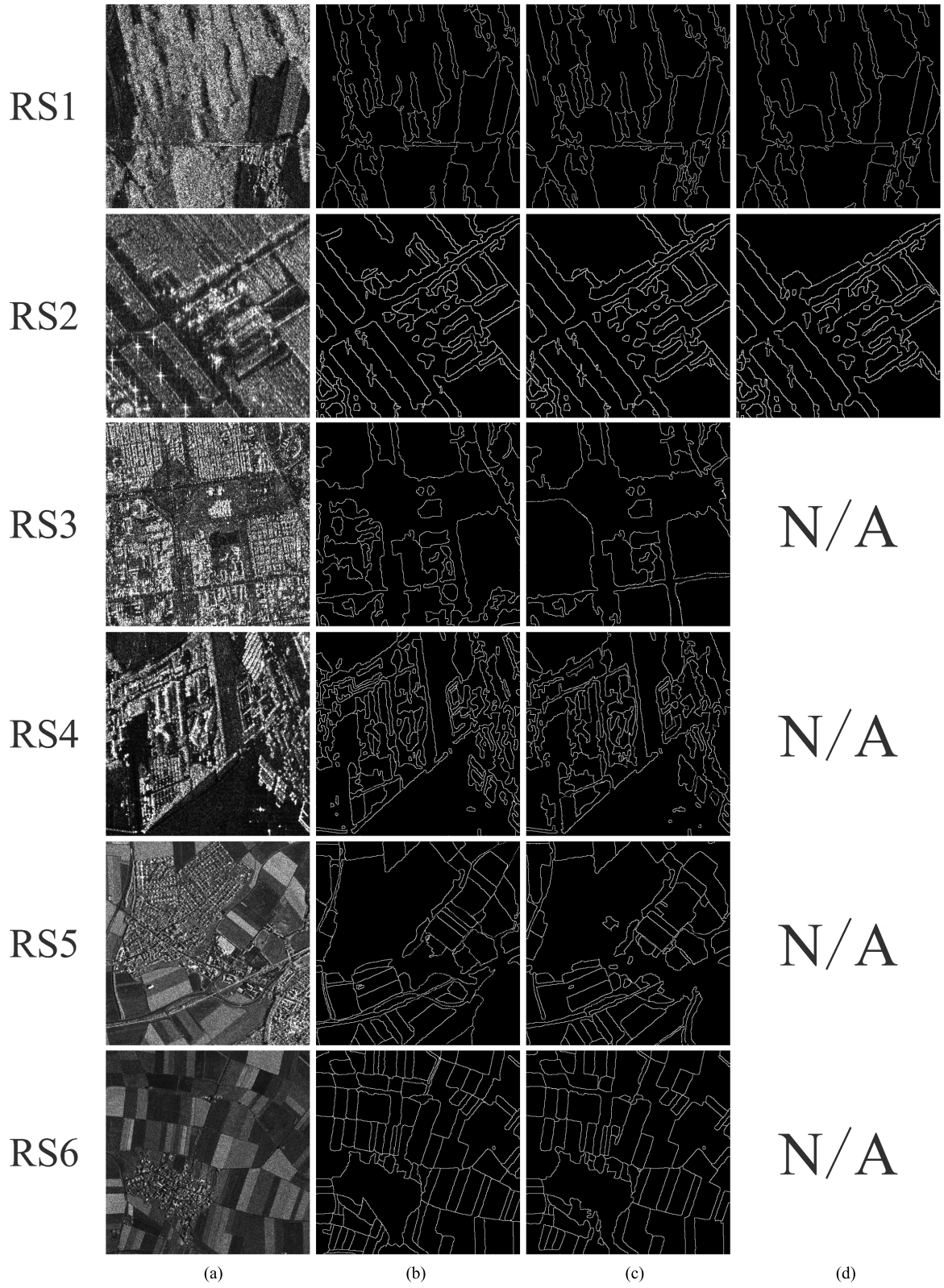

FIGURE 10. Ground Truths (GTs) of the six real SAR images generated by manual operation with different persons.

are averagely better than the other three methods, whose reason is the fact that these two methods were proposed to segment the SAR image modeled with piecewise constant scene into disjoint regions. When comparing the proposed method to the CHUMSIS and the IRGS methods for processing cartoon scenes C2,C3 and C4, the proposed method

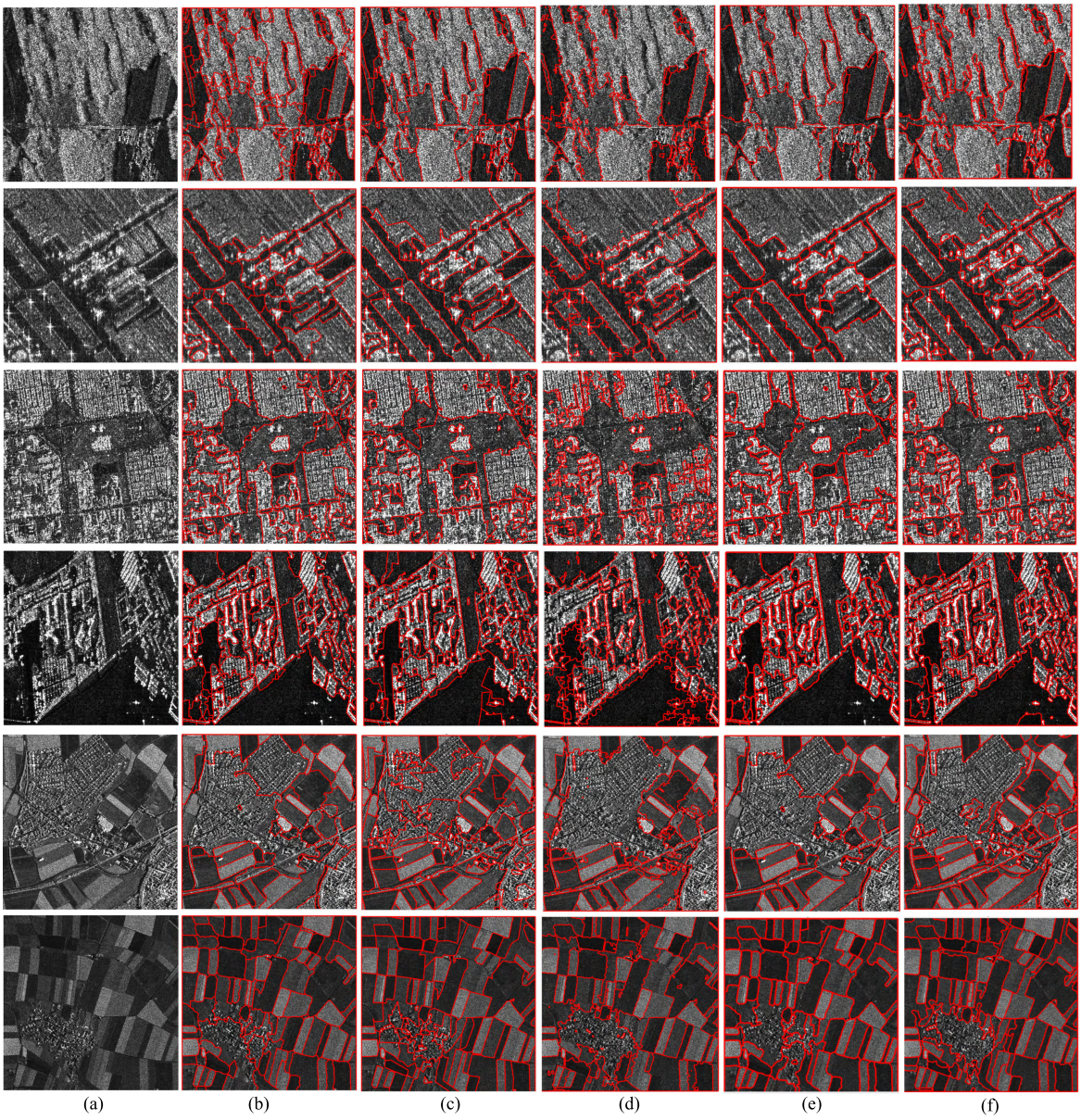

FIGURE 11. Segmentation results of real SAR images.

obtains slightly higher F-measure than the IRGS method and comparable F-measure with the CHUMSIS method.

Table 3 gives three region assessment indexes on synthetic and simulated SAR images. From Table 3, we can see that the proposed method obtains better PRI and VI indexes than the other comparing methods at most cases. And the cov. indexes obtained by these five methods for simulated SAR images are comparable.

2) REAL SAR IMAGES

In order to evaluate the performance of a method using P-R framework on real SAR images, the ground truths (GTs) of the six real SAR images used in this paper are obtained manually by different persons. Specifically, the GTs of each one of these six real SAR images are labeled by more than one person with their own interpretation for the image. The ground truths of the six real SAR images are shown in Fig. 10. The precision (recall and F-measure) of a segmentation result produced by a certain method are average values of the

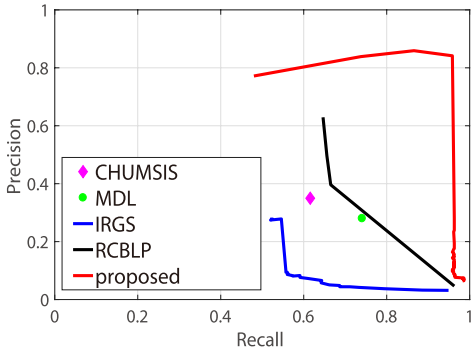

FIGURE 12. P-R curve comparison of the five methods for the synthetic SAR image S1 with GT.

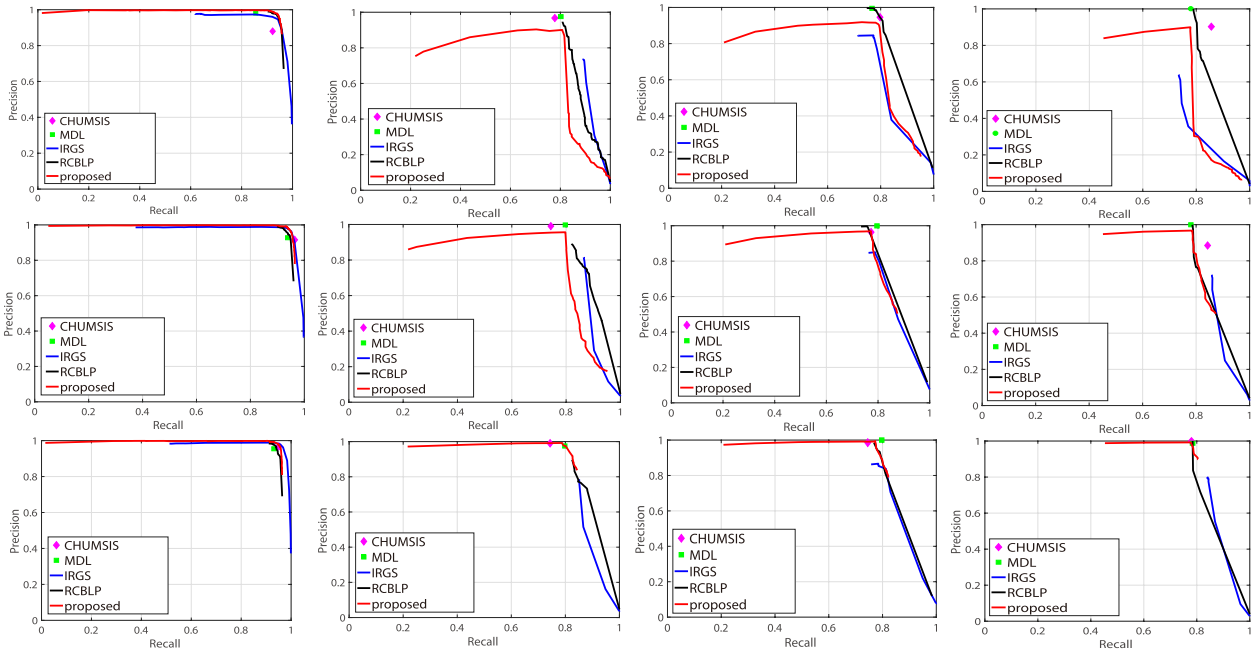

FIGURE 13. P-R curve comparisons of the five methods for the single-look, two-look and four-looks (from top to bottom row) simulated SAR images generated by the four cartoon scenes (C1, C2, C3 and C4) with GTs.

TABLE 2. Comparisons of recalls(R), Precisions(P), and F-measures(F) of the five methods for the synthetic and simulated SAR images (where the bold fonts stand for the best F-measures).

number of look	SAR image	CHUMSIS			MDL			IRGS			RCBLP			proposed		
		R	P	F	R	P	F	R	P	F	R	P	F	R	P	F
N/A	S1	0.62	0.35	0.45	0.74	0.28	0.41	0.55	0.28	0.37	0.65	0.63	0.64	0.96	0.84	**0.90**
Look1	C1	0.92	0.88	0.90	0.86	0.98	0.91	0.94	0.95	0.94	0.94	0.98	**0.96**	0.94	0.98	**0.96**
	C2	0.78	0.97	0.86	0.80	0.98	**0.88**	0.89	0.74	0.81	0.81	0.95	0.87	0.81	0.90	0.85
	C3	0.80	0.95	0.87	0.77	1.00	**0.87**	0.77	0.85	0.81	0.78	0.98	**0.87**	0.79	0.91	0.85
	C4	0.86	0.90	**0.88**	0.78	1.00	**0.88**	0.73	0.64	0.68	0.79	1.00	**0.88**	0.78	0.90	0.83
Look2	C1	0.96	0.92	0.94	0.94	0.93	0.93	0.94	0.98	0.96	0.92	0.98	0.95	0.94	0.99	**0.96**
	C2	0.74	0.99	0.85	0.80	1.00	0.89	0.87	0.82	0.84	0.82	**0.89**	0.85	0.80	0.96	0.87
	C3	0.77	0.96	0.86	0.80	1.00	**0.89**	0.79	0.85	0.82	0.76	1.00	0.86	0.77	0.97	0.86
	C4	0.84	0.88	0.86	0.78	1.00	**0.88**	0.86	0.72	0.79	0.79	1.00	**0.88**	0.79	0.97	0.87
Look4	C1	0.95	0.97	0.96	0.93	0.95	0.94	0.95	0.98	**0.96**	0.94	0.97	0.95	0.95	0.98	**0.96**
	C2	0.74	0.99	0.85	0.80	0.97	**0.88**	0.85	0.79	0.82	0.83	0.90	0.86	0.80	0.98	**0.88**
	C3	0.74	0.99	0.85	0.80	1.00	**0.89**	0.81	0.84	0.82	0.77	0.98	0.86	0.77	0.99	0.87
	C4	0.78	1.00	**0.88**	0.78	0.99	0.87	0.84	0.80	0.82	0.78	1.00	**0.88**	0.78	0.99	0.87

TABLE 3. Region assessment indexes on synthetic and simulated SAR images with different numbers of looks (The bold fonts denote the best indexes).

number of look	SAR image	CHUMSIS			MDL			IRGS			RCBLP			proposed		
		PRI	VI	Cov	PRI	VI	Cov	PRI	VI	Cov	PRI	VI	Cov	PRI	VI	Cov
N/A	S1	0.95	0.85	0.83	0.92	0.94	0.80	0.89	0.86	0.74	0.96	0.57	0.88	**1.00**	**0.06**	**0.98**
Look1	C1	0.13	4.62	0.25	0.26	2.16	0.34	0.23	2.60	0.24	0.23	2.56	0.29	**1.00**	**0.00**	**0.57**
	C2	0.91	0.66	0.76	**1.00**	0.09	**0.99**	0.99	0.24	0.96	**1.00**	0.12	**0.99**	**1.00**	**0.07**	0.98
	C3	0.88	0.82	0.71	0.96	0.49	**0.92**	0.96	0.49	0.89	0.96	0.50	0.91	**0.97**	**0.37**	0.91
	C4	**1.00**	0.08	**0.99**	**1.00**	0.07	**0.99**	0.95	0.49	0.88	**1.00**	0.08	**0.99**	**1.00**	**0.02**	**0.99**
Look2	C1	0.12	4.33	0.20	0.29	2.01	0.34	0.47	1.43	0.47	0.23	2.56	0.29	**1.00**	**0.00**	**0.57**
	C2	0.92	0.60	0.76	**1.00**	0.06	**1.00**	**1.00**	0.10	0.98	**1.00**	0.14	0.98	**1.00**	**0.03**	0.99
	C3	0.78	1.22	0.51	**0.97**	0.41	**0.92**	**0.97**	0.41	0.90	0.96	0.50	0.91	**0.97**	**0.33**	0.91
	C4	**1.00**	0.07	**0.99**	**1.00**	0.06	**0.99**	0.99	0.11	0.98	**1.00**	0.08	**0.99**	**1.00**	**0.02**	**0.99**
Look4	C1	0.15	3.64	0.24	0.27	2.24	0.34	0.26	2.16	0.29	0.27	2.34	0.34	**1.00**	**0.00**	**0.57**
	C2	0.92	0.60	0.76	**1.00**	0.05	**1.00**	**1.00**	0.09	0.98	**1.00**	0.15	0.98	**1.00**	**0.02**	0.99
	C3	0.88	0.74	0.72	**0.97**	0.37	**0.93**	**0.97**	0.37	0.91	0.96	0.50	0.91	**0.97**	**0.31**	0.92
	C4	**1.00**	**0.01**	**0.99**	**1.00**	0.06	**0.99**	**1.00**	0.06	0.98	**1.00**	0.07	**0.99**	**1.00**	0.02	**0.99**

precisions (recalls and F-measures, respectively) calculated by using the segmentation result to match every GT of the image.

Fig. 14 plots the P-R curve comparisons of the five methods for these six real SAR images and Table 4 gives their precisions, recalls and F-measures at the best hierarchy in the hierarchical segmentation tree. Fig. 14 and Table 4 indicate that, in most cases, the proposed method achieves better P-R curve and F-measure than the other comparing methods, which means that the precision of the edge location of the

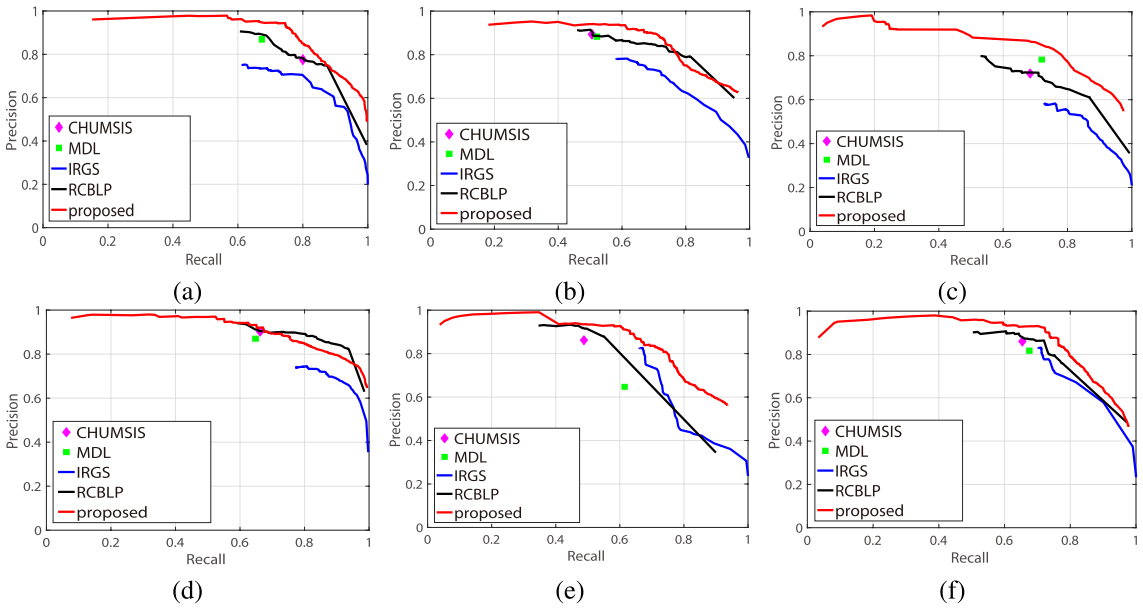

FIGURE 14. P-R curve comparisons of the five methods for the six real SAR images with GTs.

TABLE 4. Comparisons of recalls(R), Precisions(P), and F-measures(F) of the five methods for the six Real SAR images (where the bold fonts stand for the best F-measures).

	CHUMSIS			MDL			IRGS			RCBLP			proposed		
	R	P	F	R	P	F	R	P	F	R	P	F	R	P	F
RS1	0.80	0.78	0.79	0.67	0.87	0.76	0.80	0.71	0.75	0.87	0.75	0.81	0.75	0.94	**0.83**
RS2	0.51	0.89	0.65	0.52	0.88	0.66	0.72	0.72	0.72	0.81	0.79	**0.80**	0.73	0.87	**0.80**
RS3	0.68	0.72	0.70	0.72	0.78	0.75	0.76	0.58	0.66	0.87	0.61	0.72	0.78	0.80	**0.79**
RS4	0.66	0.90	0.76	0.65	0.87	0.74	0.86	0.72	0.78	0.93	0.83	**0.88**	0.91	0.79	0.85
RS5	0.49	0.86	0.62	0.61	0.65	0.63	0.67	0.83	0.74	0.62	0.77	0.69	0.74	0.81	**0.77**
RS6	0.65	0.86	0.74	0.68	0.82	0.74	0.71	0.83	0.77	0.72	0.86	0.79	0.76	0.87	**0.81**

TABLE 5. Region assessment indexes on real SAR images with different scenes (The bold fonts denote the best indexes).

	CHUMSIS			MDL			IRGS			RCBLP			proposed		
	PRI	VI	Cov	PRI	VI	Cov	PRI	VI	Cov	PRI	VI	Cov	PRI	VI	Cov
RS1	0.87	3.28	0.36	0.88	2.31	0.50	0.90	2.44	0.57	0.88	2.12	0.59	**0.92**	**1.57**	**0.76**
RS2	0.88	2.45	0.53	0.87	2.66	0.42	0.87	2.93	0.51	0.88	2.34	0.55	**0.90**	**1.70**	**0.78**
RS3	0.87	2.98	0.45	0.85	2.59	0.50	0.87	2.80	0.50	0.86	2.41	0.55	**0.92**	**1.53**	**0.74**
RS4	0.88	2.91	0.45	0.85	3.29	0.34	0.85	3.69	0.34	0.91	2.38	0.59	**0.93**	**1.89**	**0.77**
RS5	0.84	2.45	0.48	0.83	2.87	0.44	0.88	1.96	0.64	0.88	2.06	0.64	**0.89**	**1.52**	**0.76**
RS6	0.97	1.74	0.58	0.97	1.70	0.58	**0.98**	1.53	0.67	**0.98**	1.65	0.69	**0.98**	**1.05**	**0.80**

segmentation results produced by the proposed method is higher than ones generated by the other comparing methods, which is coincident with visually results shown in Fig. 11.

Table 5 illustrates three region assessment indexes on real SAR images for different methods, which shows that the proposed method achieves the best values in these five methods. Table 5 indicates that the regions produced by the proposed method are closer to the GT than the ones generated by the other comparing methods.

VII. CONCLUSION

This paper has proposed a SAR image segmentation method utilizing hierarchical region merging with a gradually increased orientated edge strength weighted Kuiper's distance. By using the proposed Bhattacharyya coefficient-based (BHC-based) edge information detector, the BHC-based watershed transform can obtain a high quality initial partition results with a small number of regions and little under-segmentation. This forms the basis of high quality segmentation results of the proposed method. The Kuiper's distance-based SSM was used to measure the similarity of a pair of adjacent regions and was multiplied by the proposed gradually increased orientated edge strength penalty (GIOESP). Then, a new hierarchical region-merging criterion was obtained. The main contributions of this paper are summarized as follows: 1) Bhattacharyya coefficient based edge detector has been proposed to estimate the ESM of a SAR image with strong speckle noise and rich texture

information; 2) based on the estimated orientated Bhattacharyya ESM, a novel Gradually Increasing Orientated Edge Strength Penalty (GIOESP) term has been presented to yield hierarchical segmentation results via changing the strength of the penalty term; and 3) a novel region merging cost has been proposed by using the GIOESP term to multiply the Kuiper's distance-based SSM term. A mass of experimental results using synthetic and real SAR images was made for the assessment of the proposed method. Visual and quantitative assessments show that the proposed method outperformed the four state-of-the-art methods in boundary localization and region consistency.

Furthermore, the above described experiment shows that the proposed Bhattacharyya coefficient-based edge information detector is an effective way to search for the transition between homogeneous and heterogeneous regions in a SAR image. It can be used in edge detection, feature representation, and other fields. More studies using Bhattacharyya coefficient on the SAR image will be explored in our future work.

REFERENCES

[1] F. Wang, Y. Wu, P. Zhang, Q. Zhang, and M. Li, "Unsupervised SAR image segmentation using ambiguity label information fusion in triplet Markov fields model," *IEEE Geosci. Remote Sens. Lett.*, vol. 14, no. 9, pp. 1479–1483, Sep. 2017.

[2] L. Gemme and S. G. Dellepiane, "An automatic data-driven method for SAR image segmentation in sea surface analysis," *IEEE Trans. Geosci. Remote Sens.*, vol. 56, no. 5, pp. 2633–2646, May 2018.

[3] Y. Duan *et al.*, "Hierarchical multinomial latent model with G^0 distribution for synthetic aperture radar image semantic segmentation," *IEEE Access*, vol. 6, pp. 31783–31797, 2018.

[4] F. Galland, N. Bertaux, and P. Réfrégier, "Minimum description length synthetic aperture radar image segmentation," *IEEE Trans. Image Process.*, vol. 12, no. 9, pp. 995–1006, Sep. 2003.

[5] X. Qin, S. Zhou, and H. Zou, "SAR image segmentation via hierarchical region merging and edge evolving with generalized gamma distribution," *IEEE Geosci. Remote Sens. Lett.*, vol. 11, no. 10, pp. 1742–1746, Oct. 2014.

[6] M. A. Hasnat, O. Alata, and A. Tremeau, "Joint color-spatial-directional clustering and region merging (JCSD-RM) for unsupervised RGB-D image segmentation," *IEEE Trans. Pattern Anal. Mach. Intell.*, vol. 38, no. 11, pp. 2255–2268, Nov. 2016.

[7] C. Wang, H. Zhang, L. Yang, X. Cao, and H. Xiong, "Multiple semantic matching on augmented N-partite graph for object co-segmentation," *IEEE Trans. Image Process.*, vol. 26, no. 12, pp. 5825–5839, Dec. 2017.

[8] J.-H. Syu, S.-J. Wang, and L.-C. Wang, "Hierarchical image segmentation based on iterative contraction and merging," *IEEE Trans. Image Process.*, vol. 26, no. 5, pp. 2246–2260, May 2017.

[9] Q. Yu and D. A. Clausi, "IRGS: Image segmentation using edge penalties and region growing," *IEEE Trans. Pattern Anal. Mach. Intel.*, vol. 30, no. 12, pp. 2126–2139, Dec. 2008.

[10] Q. Yu and D. A. Clausi, "SAR sea-ice image analysis based on iterative region growing using semantics," *IEEE Trans. Geosci. Remote Sens.*, vol. 45, no. 12, pp. 3919–3931, Dec. 2007.

[11] F. Wang, Y. Wu, M. Li, P. Zhang, and Q. Zhang, "Adaptive hybrid conditional random field model for SAR image segmentation," *IEEE Trans. Geosci. Remote Sens.*, vol. 55, no. 1, pp. 537–550, Jan. 2017.

[12] G. S. Xia, C. He, and H. Sun, "Integration of synthetic aperture radar image segmentation method using Markov random field on region adjacency graph," *IET Radar, Sonar Navigat.*, vol. 1, no. 5, pp. 348–353, Oct. 2007.

[13] W. Li *et al.*, "Watershed-based hierarchical SAR image segmentation," *Int. J. Remote Sens.*, vol. 20, no. 17, pp. 3377–3390, 1999.

[14] P.-L. Shui and Z.-J. Zhang, "Fast SAR image segmentation via merging cost with relative common boundary length penalty," *IEEE Trans. Geosci. Remote Sens.*, vol. 52, no. 10, pp. 6434–6448, Oct. 2014.

[15] C. J. Oliver, D. Blacknell, and R. G. White, "Optimum edge detection in SAR," *IEE Proc.-Radar, Sonar Navigat.*, vol. 143, no. 1, pp. 31–40, Feb. 1996.

[16] R. Fjortoft, A. Lopes, P. Marthon, and E. Cubero-Castan, "An optimal multiedge detector for SAR image segmentation," *IEEE Trans. Geosci. Remote Sens.*, vol. 36, no. 3, pp. 793–802, May 1998.

[17] J. Schou, H. Skriver, A. A. Nielsen, and K. Conradsen, "CFAR edge detector for polarimetric SAR images," *IEEE Trans. Geosci. Remote Sens.*, vol. 41, no. 1, pp. 20–32, Jan. 2003.

[18] R. C. P. Marques, F. N. Medeiros, and J. S. Nobre, "SAR image segmentation based on level set approach and G_A^0 model," *IEEE Trans. Pattern Anal. Mach. Intell.*, vol. 34, no. 10, pp. 2046–2057, Oct. 2012.

[19] J. Feng, Z. Cao, and Y. Pi, "Multiphase SAR image segmentation with G^0-statistical-model-based active contours," *IEEE Trans. Geosci. Remote Sens.*, vol. 51, no. 7, pp. 4190–4199, Jul. 2013.

[20] F. Galland, J.-M. Nicolas, H. Sportouche, M. Roche, F. Tupin, and P. Réfrégier, "Unsupervised synthetic aperture radar image segmentation using Fisher distributions," *IEEE Trans. Geosci. Remote Sens.*, vol. 47, no. 8, pp. 2966–2972, Aug. 2009.

[21] G. Delyon and P. Réfrégier, "SAR image segmentation by stochastic complexity minimization with a nonparametric noise model," *IEEE Trans. Geosci. Remote Sens.*, vol. 44, no. 7, pp. 1954–1961, Jul. 2006.

[22] B. N. Li, J. Qin, R. Wang, M. Wang, and X. Li, "Selective level set segmentation using fuzzy region competition," *IEEE Access*, vol. 4, pp. 4777–4788, Aug. 2016.

[23] C. Peng, S.-L. Lo, J. Huang, and A. C. Tsoi, "Human action segmentation based on a streaming uniform entropy slice method," *IEEE Access*, vol. 6, pp. 16958–16971, 2018.

[24] F. Goudail, P. Réfrégier, and G. Delyon, "Bhattacharyya distance as a contrast parameter for statistical processing of noisy optical images," *J. Opt. Soc. Amer. A, Opt. Image Sci.*, vol. 21, no. 7, pp. 1231–1240, 2004.

[25] I. B. Ayed, K. Punithakumar, and S. Li, "Distribution matching with the bhattacharyya similarity: A bound optimization framework," *IEEE Trans. Pattern Anal. Mach. Intell.*, vol. 37, no. 9, pp. 1777–1791, Sep. 2015.

[26] J. Morio, P. Refrégier, F. Goudail, P. C. Dubois-Fernandez, and X. Dupuis, "A characterization of Shannon entropy and Bhattacharyya measure of contrast in polarimetric and interferometric SAR image," *Proc. IEEE*, vol. 97, no. 6, pp. 1097–1108, Jun. 2009.

[27] A. Levinshtein, A. Stere, K. N. Kutulakos, D. J. Fleet, S. J. Dickinson, and K. Siddiqi, "TurboPixels: Fast superpixels using geometric flows," *IEEE Trans. Pattern Anal. Mach. Intell.*, vol. 31, no. 12, pp. 2290–2297, Dec. 2009.

[28] R. Achanta, A. Shaji, K. Smith, A. Lucchi, P. Fua, and S. Süsstrunk, "usstrunk, "SLIC superpixels compared to state-of-the-art superpixel methods," *IEEE Trans. Pattern Anal. Mach. Intell.*, vol. 34, no. 11, pp. 2274–2282, Nov. 2012.

[29] O. Veksler, Y. Boykov, and P. Mehrani, "Superpixels and supervoxels in an energy optimization framework," in *Proc. Eur. Conf. Comput. Vis.* Springer, 2010, pp. 211–224.

[30] G. Mori, "Guiding model search using segmentation," in *Proc. 10th IEEE Int. Conf. Comput. Vis. (ICCV)*, Oct. 2005, pp. 1417–1423.

[31] M.-Y. Liu, O. Tuzel, S. Ramalingam, and R. Chellappa, "Entropy-rate clustering: Cluster analysis via maximizing a submodular function subject to a matroid constraint," *IEEE Trans. Pattern Anal. Mach. Intell.*, vol. 36, no. 1, pp. 99–112, Jan. 2014.

[32] L. Vincent and P. Soille, "Watersheds in digital spaces: An efficient algorithm based on immersion simulations," *IEEE Trans. Pattern Anal. Mach. Intell.*, vol. 13, no. 6, pp. 583–598, Jun. 1991.

[33] E. A. Carvalho, D. M. Ushizima, F. N. Medeiros, C. I. O. Martins, R. C. Marques, and I. N. Oliveira, "SAR imagery segmentation by statistical region growing and hierarchical merging," *Digit. Signal Process.*, vol. 20, no. 5, pp. 1365–1378, 2010.

[34] S. Arisoy and K. Kayabol, "Mixture-based superpixel segmentation and classification of SAR images," *IEEE Geosci. Remote Sens. Lett.*, vol. 13, no. 11, pp. 1721–1725, Nov. 2016.

[35] R. Nock and F. Nielsen, "Statistical region merging," *IEEE Trans. Pattern Anal. Mach. Intell.*, vol. 26, no. 11, pp. 1452–1458, Nov. 2004.

[36] K. Haris, S. N. Efstratiadis, N. Maglaveras, and A. K. Katsaggelos, "Hybrid image segmentation using watersheds and fast region merging," *IEEE Trans. Image Process.*, vol. 7, no. 12, pp. 1684–1699, Dec. 1998.

[37] F. Calderero and F. Marques, "Region merging techniques using information theory statistical measures," *IEEE Trans. Image Process.*, vol. 19, no. 6, pp. 1567–1586, Jun. 2010.

[38] Y. Yang, H. Sun, and C. He, "Supervised SAR Image MPM Segmentation Based on Region-Based Hierarchical Model," *IEEE Geosci. Remote Sens. Lett.*, vol. 3, no. 4, pp. 517–521, Oct. 2006.
[39] J. Cousty, L. Najman, Y. Kenmochi, and S. Guimarães, "Hierarchical segmentations with graphs: Quasi-flat zones, minimum spanning trees, and saliency maps," *J. Math. Imag. Vis.*, vol. 60, no. 4, pp. 479–502, 2018.
[40] B. Perret, J. Cousty, S. J. F. Guimaraes, and D. S. Maia, "Evaluation of hierarchical watersheds," *IEEE Trans. Image Process.*, vol. 27, no. 4, pp. 1676–1688, Apr. 2018.
[41] A. Savitzky and M. J. E. Golay, "Smoothing and differentiation of data by simplified least squares procedures," *Anal. Chem.*, vol. 36, no. 8, pp. 1627–1639, 1964.
[42] W. H. Press, S. A. Teukolsky, W. T. Vetterling, and B. P. Flannery, *Numerical Recipes: The Art of Scientific Computing*, vol. 3, 3rd ed. Cambridge, U.K.: Cambridge Univ. Press, 2007.
[43] M. A. Stephens, "Use of the Kolmogorov–Smirnov, Cramer–Von Mises and related statistics without extensive tables," *J. Roy. Stat. Soc. B (Methodol.)*, vol. 32, no. 1, pp. 115–122, 1970.
[44] H. Yu, X. Zhang, S. Wang, and B. Hou, "Context-based hierarchical unequal merging for SAR image segmentation," *IEEE Trans. Geosci. Remote Sens.*, vol. 51, no. 2, pp. 995–1009, Feb. 2013.
[45] P. Arbeláez, M. Maire, C. Fowlkes, and J. Malik, "Contour detection and hierarchical image segmentation," *IEEE Trans. Pattern Anal. Mach. Intell.*, vol. 33, no. 5, pp. 898–916, May 2011.

ZEJUN ZHANG received the B.S. and M.S. degrees in computer science from Guizhou University, Guiyang, China, in 2007 and 2010, respectively, and the Ph.D. degree in electronic engineering from Xidian University, Xi'an, China, in 2014. He is currently a Lecturer with the College of Computer and Information Sciences, Fujian Agriculture and Forestry University, Fuzhou, China. His current research interests include pattern recognition and synthetic aperture radar image processing.

XIONG PAN received the B.S. degree in computer science from Shanxi University, Taiyuan, China, in 2017. He is currently pursuing the M.S. degree in computer science with Fujian Agriculture and Forestry University, Fuzhou, China. His current research interest includes digital image processing.

LI CHENG is currently an Associate Professor with the College of Computer and Information Sciences, Fujian Agriculture and Forestry University, Fuzhou, China. Her research interests include pattern recognition and natural language processing.

SHIHUA ZHAN received the B.S. degree in industrial electric automation from Fuzhou University, Fuzhou, China, in 1990. He is currently an Associate Professor with the College of Computer and Information Science, Fujian Agriculture and Forestry University, Fuzhou. His current research interests include computational intelligence and network security.

HUABING ZHOU received the Ph.D. degree in control science and engineering from the Huazhong University of Science and Technology, Wuhan, China, in 2012.

He is currently an Assistant Professor with the School of Computer Science and Engineering, Wuhan Institute of Technology, Wuhan. His research interests include remote sensing image analysis, computer vision, and intelligent robotics.

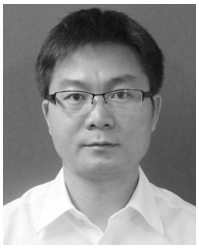

RIQING CHEN received the B.Eng. degree in communication engineering from Tongji University, China, in 2001, the M.Sc. degree in communications and signal processing from Imperial College London, U.K., in 2004, and the Ph.D. degree in engineering science from the University of Oxford, U.K., in 2010. Since 2014, he has been a Professor and a M.S. Supervisor with the College of Computer and Information Science, Fujian Agriculture and Forestry University, Fuzhou, China. His current research interests include big data and visualization, cloud computing, consumer electronics, flash memory, wireless sensor networking, and image processing.

CHANGCAI YANG received the M.S. degree in control theory and control engineering from China Three Gorges University, China, in 2008, and the Ph.D. degree in pattern recognition and intelligent systems from the Huazhong University of Science and Technology (HUST), China, in 2012.

From 2012 to 2014, he held a Postdoctoral position with HUST. Since 2016, he has been an Associate Professor and a M.S. Supervisor with the College of Computer and Information Science, Fujian Agriculture and Forestry University, Fuzhou, China. He has published more than 30 papers. His research interests include computer vision, image processing, and point set registration.

CHANGYING WANG received the Ph.D. degree in computer software and theory from North West University, Xi'an, in 2006. He is currently a Professor with the College of Computer and Information Science, Fujian Agriculture and Forestry University, Fuzhou, China. His current research interests include computer vision, computational intelligence, and parallel computing.

YAOHAI LIN is currently an Associate Professor with the College of Computer and Information Sciences, Fujian Agriculture and Forestry University, Fuzhou, China. His research interests include intelligent information processing, image processing, and computational imaging.

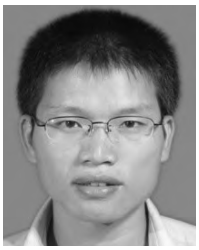

JIAXIANG LIN received the Ph.D. degree in communication and information system from Fuzhou University, China, in 2010. He is currently a Lecturer with the College of Computer and Information Sciences, Fujian Agriculture and Forestry University, Fuzhou, China. He has hosted four national, provincial, and ministerial level research projects, authored over 40 referred journal and conference papers, and holds two patents of invention. His research interests include spatial data mining, artificial intelligence, and big data.